

Effective Quantum Dimer Model for the Kagome Heisenberg Antiferromagnet: Nearby Quantum Critical Point and Hidden Degeneracy

Didier Poilblanc,¹ Matthieu Mambrini,¹ and David Schwandt¹

¹*Laboratoire de Physique Théorique, CNRS and Université de Toulouse, F-31062 Toulouse, France*

(Dated: September 1, 2021)

The low-energy singlet dynamics of the Quantum Heisenberg Antiferromagnet on the Kagome lattice is described by a quantitative Quantum Dimer Model. Using advanced numerical tools, the latter is shown to exhibit Valence Bond Crystal order with a large 36-site unit cell and hidden degeneracy between even and odd parities. Evidences are given that this groundstate lies in the vicinity of a \mathbb{Z}_2 dimer liquid region separated by a Quantum Critical Point. Implications regarding numerical analysis and experiments are discussed.

PACS numbers: 74.20.Mn, 67.80.kb, 75.10.Jm, 74.75.Dw, 74.20.Rp

The Kagome lattice, a two-dimensional corner-sharing array of triangles shown on Fig. 1(a), is believed to be one of the most frustrated lattices leading to finite entropy in the ground-state (GS) of the classical Heisenberg model [1]. Hence, the Quantum S=1/2 Heisenberg Antiferromagnet (QHAF) on the Kagome lattice is often considered as the paradigm of quantum frustrated magnetism [2] where, in contrast to conventional broken symmetry phases of spin systems (as e.g. magnetic phases), exotic *quantum liquids or crystals* could be realized. Among the latter, the algebraic (gapless) spin liquid is one of the most intriguing candidate [3].

The herbertsmithite [4] compound is one of the few experimental realizations of the S=1/2 Kagome QHAF. The absence of magnetic ordering [5] down to temperatures much smaller than the typical energy scale of the exchange coupling J suggests that, indeed, intrinsic properties of the Kagome QHAF can be observed, even-though Nuclear Magnetic Resonance and Electron Spin Resonance reveal a small fraction of non-magnetic impurities [6] and small Dzyaloshinsky-Moriya anisotropy [7]. So far, the nature of the non-magnetic phase is unknown and confrontation to new theoretical ideas have become necessary. Alternatively, ultra-cold atoms loaded on an optical lattice with tunable interactions might enable to also explore the physics of extended Kagome QHAF [8].

The QHAF on the Kagome lattice has been addressed theoretically by Lanczos Exact Diagonalization (LED) of small clusters [9, 10]. Despite the fact that the accessible cluster sizes remain very small, these data are consistent with a finite spin gap and an exponential number of singlets within the gap, in agreement with a recent Density Matrix Renormalization Group study [11]. In addition, an analysis of the four-spin correlations pointed towards a *short-range* dimer liquid phase [12]. Alternatively, a large-N approach [13] and various mappings to low-energy effective Hamiltonians within the singlet subspace [14–16] have suggested the formation of translation-symmetry breaking Valence Bond Crystals (VBC). Recently, recent series expansions around the dimer limit [17] showed that a 36-site VBC unit cell is preferred (see Fig 1(a)). In this context, the interpretation of the LED low-energy singlet spectrum remains problematic [18].

In this Letter, we use a quantitative dimer-projected effec-

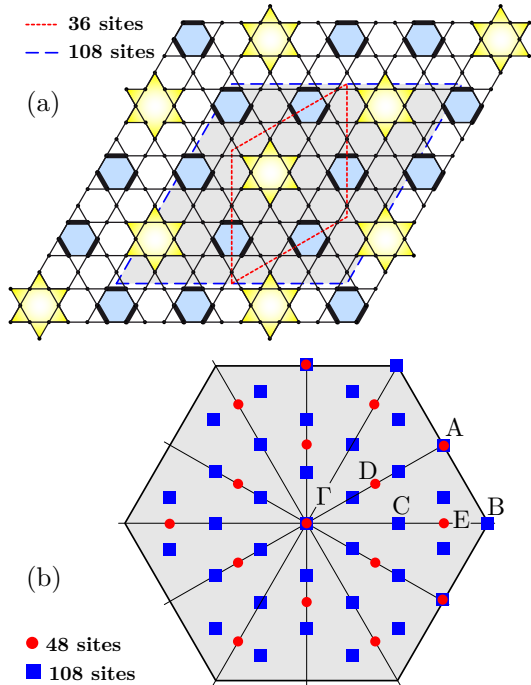


FIG. 1: (color online) (a) Sketch of the 36-site VBC on the Kagome lattice showing “perfect hexagons” and (yellow) “star” resonances. Its unit cell is delimited by dashed (red) lines. The extension of the 108-site cluster (which fits exactly three 36-site cells) is (lightly) shaded and delimited by long-dashed (blue) lines. Hardcore dimers (formed by two neighboring spin- $\frac{1}{2}$) are located on the bonds (only shown on the shaded hexagons). (b) First Brillouin zone and available momenta (labeling consistent with Ref. [18]).

tive model to describe the low-energy singlet subspace of the Kagome QHAF. This is based on a controlled loop expansion [19] along the lines initiated by Rohksar and Kivelson (RK) [20] in the context of High-Temperature Superconductivity and by Zeng and Elser [21] (ZE) for the Kagome lattice. LED of the effective model enable to reach unprecedented sizes of periodic clusters which can accommodate a finite number of candidate VBC unit cells. The major results are (i) the numerical evidence of VBC order with a large 36-

site unit cell and a hidden degeneracy, (ii) the vicinity of a \mathbb{Z}_2 dimer liquid region separated by a Quantum Critical Point. Such results transposed to the original QHAF could explain some of its former puzzling numerical findings.

Model – The method consists in projecting the QHAF, $\mathcal{H} = J \sum_{\langle i,j \rangle} \mathbf{S}_i \cdot \mathbf{S}_j$, i and j being nearest neighbor (NN) lattice sites, into the manifold formed by NN Valence Bond (VB) coverings, an approximation shown to be excellent for the Kagome lattice [21–23]. A transformation is then performed that turns the non-orthogonal VB basis into an orthogonal Quantum Dimer basis. Overlaps between NN VB states can be written [24] (up to a sign) as α^{N-2n_l} where N is the system size, n_l the number of loops obtained by superimposing the two configurations, and $\alpha = 1/\sqrt{2}$. This enables a systematic expansion in powers of α involving at order α^{2p} ($p \geq 2$) loops of sizes up to $\mathcal{L} = 2p + 2$ [19, 25] leading to a generalized Quantum Dimer Model (QDM) which, restricting to loops encircling only single hexagons, reads

$$\mathcal{H}_{\text{eff}} = -J_6 \text{ (hexagon)} - J_8 \left(\text{ (hexagon)} + \text{ (hexagon)} + \text{ (hexagon)} \right) \quad (1)$$

$$\begin{aligned} & -J_{10} \left(\text{ (hexagon)} + \text{ (hexagon)} + \text{ (hexagon)} \right) - J_{12} \text{ (hexagon)} \\ & + V_6 \text{ (hexagon)} + V_8 \left(\text{ (hexagon)} + \text{ (hexagon)} + \text{ (hexagon)} \right) \quad (2) \\ & + V_{10} \left(\text{ (hexagon)} + \text{ (hexagon)} + \text{ (hexagon)} \right) + V_{12} \text{ (hexagon)}, \end{aligned}$$

where a sum over all the hexagons of the lattice of Fig. 1(a) is implicit. Kinetic terms (1) promote cyclic permutations of the dimers around the loops and diagonal terms (2) count the numbers of “flippable” loops. Here we use the approximate values (14-th order), $V_6 = 0.2$, $V_8 = 0.032$, $V_{10} = V_{12} = 0$, $J_6 = -0.8$, $J_8 = 0.251$, $J_{10} = -0.063$, $J_{12} = 0$ (in units of J). Note that the kinetic processes $J_{\mathcal{L}}$ are quite close to ZE [21] initial lowest-order estimates, $J_6 = -3/4$, $J_8 = 1/4$ and $J_{10} = -1/16$, a good sign of convergence of the expansion. Very importantly, we also include here the potential $V_{\mathcal{L}}$ terms which appear in our expansion scheme only at order $2(\mathcal{L} - 2)$ but play a major role. Note that an exact resummation of the weights of (1), (2) up to all orders can be carried out (leading to tiny deviations) and that the “star” amplitudes J_{12} and V_{12} vanish at all orders [19].

Symmetry analysis – Although the generalized QDM () bears a sign problem, it can be addressed by LED of periodic $3 \times L \times L$ clusters which possess all the infinite lattice symmetries and L^2 unit cells. We shall consider $L = 4$ and $L = 6$ corresponding to the 48-site and 108-site clusters (see Fig. 1(a)), a tremendous improvement in terms of system size compared to the original QHAF, and use all available lattice symmetries (see available momenta in Fig. 1(b)) to block-diagonalize the Hamiltonian in its irreducible representations (IR) [26]. We further make use of a topological symmetry which splits the Hilbert space into 4 topological sectors (TS) $\{n_1, n_2, n_3\}$, where $n_{\alpha} = 0$ (1) for an even (odd) number of

dimers cut by each crystal axis α enclosing the torus [27].

VBC	Γ	A	B	C	D	E
$\mathcal{N} = 12$	$(+, +, \pm)$	$(\times, +, \pm)$				
$\mathcal{N} = 36$	$(+, +, \pm)$	$(\times, +, \pm)$	$(+, \times, \pm)$	(\times, \times, \pm)		
$\mathcal{N} = 48$	$(+, +, \pm)$	$(\times, +, \pm)$			(\times, \times, \pm)	(\times, \times, \pm)
\mathbb{Z}_2	$(+, +, +)$					

TABLE I: Quantum numbers of the GS multiplet for VBC with \mathcal{N} -site cells ($\mathcal{N} = 3 \times m \times m$ or $\mathcal{N} = 3 \times n\sqrt{3} \times n\sqrt{3}$) and degeneracy $\mathcal{N}/3$. The letters refer to the momenta of Fig. 1. Invariance under $2\pi/3$ rotations ($r_3 = +$) and parity under inversion ($r_2 = \pm$) and/or reflection about the momentum direction (σ) are denoted as (r_3, r_2, σ) consistently with Ref. [18]. $\sigma = \pm$ corresponds to even or odd GS and “ \times ” means “symmetry not relevant”. The \mathbb{Z}_2 dimer liquid (last line) GS in TS^* is degenerate with the other TS GS [27].

An analysis of the low-energy spectrum and a careful inspection of its quantum numbers provide invaluable informations on the nature of the GS. For a VBC breaking discrete lattice symmetries, a multiplet structure is expected giving rise in the thermodynamic limit to a degenerate GS separated by a gap from the rest of the spectrum. We list in Table I the quantum numbers of the GS multiplet for the most popular VBC in the literature.

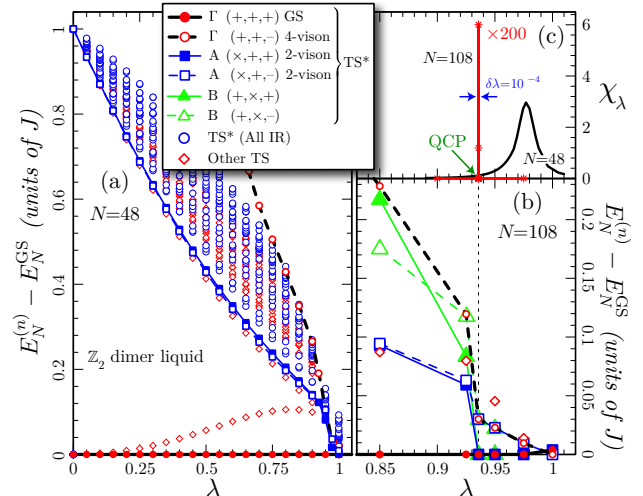


FIG. 2: (color online) (a) Complete low-energy excitation spectrum of the 48-site cluster as a function of the parameter λ (see text). The lowest 25 levels are displayed in each TS (see [27]) using different symbols/colors. The 2-vison (blue lines) and 4-vison (dashed black line) gaps vanish around $\lambda = 1$. (b) Close-up around $\lambda = 1$ showing the excitation-energy of the lowest level of the most relevant IR (see Table I) of the 108-site cluster: a QCP is identified from (i) a collapse of these excitations (b) and (ii) a very sharp peak in χ_{λ} (c) (data for $N = 108$ divided by 200 to fit the scale). Note the transition is far more abrupt for $N = 108$ than for $N = 48$ (c).

Quantum Critical Point – The QDM with only kinetic processes of equal amplitudes, $J_6 = J_8 = J_{10} = J_{12} (= 1/4)$

provides an exactly solvable model [29] \mathcal{H}_{RK} with a gapped \mathbb{Z}_2 dimer liquid GS with short-range dimer correlations, similarly to the RK-point of the triangular QDM [30]. Interestingly, the first excitations (of energy J) correspond to pairs of (localized) topological vortices (visons). It is tempting to construct a simple interpolation $\mathcal{H}(\lambda) = \lambda\mathcal{H}_{\text{eff}} + (1-\lambda)\mathcal{H}_{RK}$ between this known limit and the effective model (1), (2). Its low-energy spectrum on the 48-site and 108-site clusters are shown as a function of λ in Fig. 2(a) and Fig. 2(b), respectively. In the 48-site cluster, a high density of low-energy levels accumulate just above the GS at $\lambda \sim 1$. This strongly suggests the vicinity of a Quantum Critical Point (QCP) characterized by vortex (vison) condensation as in the triangular QDM [31]. A closer look around $\lambda = 1$ on the larger cluster reveals a sudden collapse of the low-energy excitations, clearly before $\lambda = 1$. Remarkably, as shown in Fig. 2(c), this collapse coincides exactly with a very sharp peak of the second derivative of GS energy [28] $\chi_\lambda = -\partial^2(E_N^{\text{GS}}/N)/\partial\lambda^2$, enabling to locate the QCP at $\lambda_{\text{QCP}} \sim 0.9357$. Note that the even-parity ($\sigma = +$) multi-vison excitations at momenta K_A and K_B merge with the GS precisely at λ_{QCP} (see below).

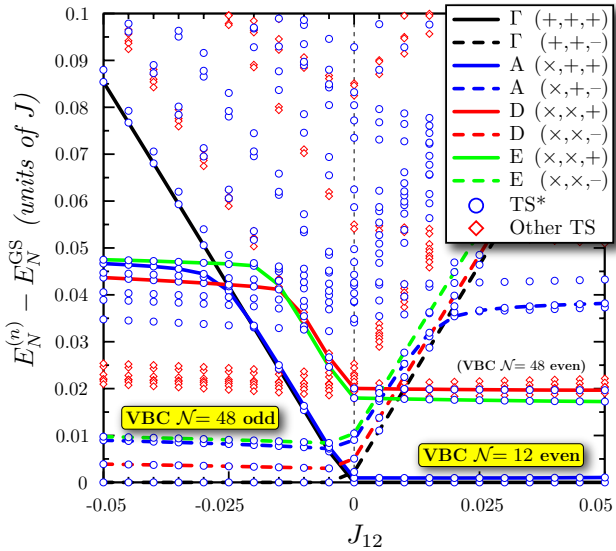


FIG. 3: (color online) Complete low-energy excitation spectrum of the 48-site cluster as a function of J_{12} . The lowest 25 levels are displayed in each TS (same symbols as Fig. 2(a)). The quantum numbers of the 4 lowest energy states for $J_{12} < 0$ and $J_{12} > 0$ are provided using different line types.

VBC and hidden degeneracy – Next, to identify the ordered phase for $\lambda > \lambda_{\text{QCP}}$ we add a finite star resonance amplitude J_{12} to H_{eff} . As seen in Figs. 3 and 4, this term has a crucial role. In fact, $J_{12} = 0$ is highly singular, with a (almost exact) degeneracy between odd ($\sigma = -$) and even ($\sigma = +$) states. Physically, we believe it is related to the hidden Ising variables (introduced in Ref. 17) associated to the resonance parities of stars (see Fig. 1(a) for the 36-site VBC). Incidentally, it is remarkable that our effective model picks up such a feature via a vanishing effective J_{12} . For finite but still very small J_{12} , this

degeneracy is lifted (favoring a “ferromagnetic” Ising configuration) allowing to characterize any candidate VBC (which should exist with both parity) from its lowest energy states.

For the 48-site cluster, a close inspection of the associated quantum numbers and a comparison with Table I suggest a VBC with a 48-site (12-site) unit cell for $J_{12} < 0$ ($J_{12} > 0$). For $J_{12} > 0$ slow fluctuations towards the pattern of a $N = 48$ VBC are signaled by the presence of intermediate mid-gap states. Note that the lowest-energy excitations in the other TS (red lozenges) which barely depend on J_{12} set roughly the (very small) VBC gap scale. Also, the high-density of levels within a small energy window of $\sim 0.1J$ above the GS is reminiscent of the singlet sector of the QHAF [18].

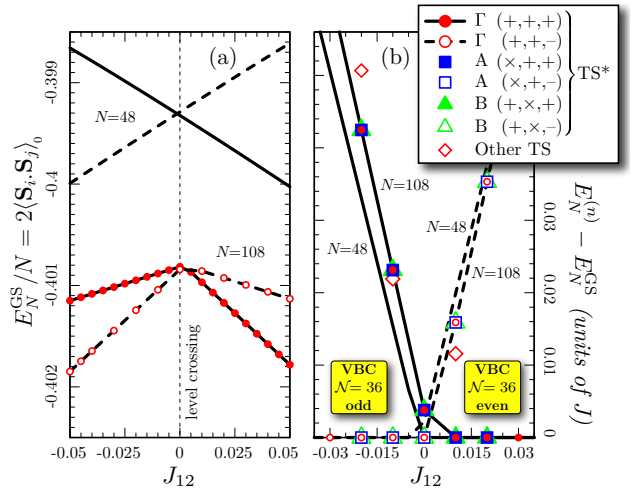


FIG. 4: (color online) (a) GS energies *per site* versus J_{12} for $K = K_\Gamma$ and $\sigma = \pm$. The minimum defines the absolute GS energy E_N^{GS}/N . Data for 48 sites (lines) and 108 sites (circles) are shown. An energy shift and scale transformation $E_N \rightarrow \frac{3}{4}(E_N - N/2)$ allow a direct comparison with twice the bond-energy of the QHAF. (b) Same as Fig. 2(b) but as a function of J_{12} and compared to the $N=48$ excitation at the Γ -point (full lines). Note the splittings between Γ , A and B levels of a few $10^{-8} J$ are invisible at this scale.

A similar analysis on the larger 108-site cluster [26] provides definite evidence in favor of the 36-site (degenerate) VBC schematically depicted in Fig. 1(a), for $\lambda > \lambda_{\text{QCP}}$. First, Fig. 4(a) shows a kink at $J_{12} = 0$ of the GS energy *per site*, coinciding with the crossing of two GS of opposite parity and leading to almost the same slope discontinuity as for $N = 48$ (size effects are small). As for $N = 48$, this, in fact, corresponds to the level crossings of two *groups of quasi-degenerate GS* with opposite parities as shown in Fig. 4(b). We note an extremely fast decrease with N of the gaps between the A and Γ quasi-degenerate GS common to both clusters (a few $10^{-3} J$ for $N = 48$ to less than $10^{-7} J$ for $N = 108$). Furthermore, the fact that a new state with momentum K_B (not allowed for $N = 48$) belongs to these two groups of quasi-degenerate GS definitely points toward a $N = 36$ unit cell [32] (which does not fit $N = 48$). This is further supported by the values of the average number N_C of

flippable length- \mathcal{L} loops compared in Table II to their values in VBC proposed in the literature.

Groundstates	N_6/N_H	N_8/N_H	N_{10}/N_H	N_{12}/N_H
$N = 108; J_{12} = 0.01$	0.154	0.274	0.491	0.081
$N = 108; J_{12} = -0.01$	0.153	0.275	0.492	0.080
$3 \times 2 \times 2$ [14]	0	0.75	0	0.25
$3 \times 2\sqrt{3} \times 2\sqrt{3}$ [13, 15, 17]	0.167	0.25	0.5	0.083
\mathbb{Z}_2 dimer liquid [29]	1/32	15/32	15/32	1/32

TABLE II: Average number $N_{\mathcal{L}}$ of flippable length- \mathcal{L} loops normalized to the total number N_H of hexagons. The last 3 lines correspond to the "frozen" limit of VBC and to the \mathbb{Z}_2 dimer-liquid.

In summary, we introduced a generalized QDM to describe the low-energy physics of the QHAF on the Kagome lattice. In contrast to the latter, its groundstate properties can be addressed by numerical simulations with unprecedented accuracy for a frustrated quantum magnet. In particular, we provide evidence of (i) a 36-site VBC order (with hidden degeneracy), in agreement with recent series expansion [17], and (ii) the vicinity of a QCP towards a topological \mathbb{Z}_2 dimer-liquid (cf. schematic phase diagram on Fig. 3 of Ref. 19). Interestingly, a double Chern-Simons field-theory [33] also describes such a Quantum Critical Point. The above remarkable features of the generalized QDM transposed to the QHAF would resolve mysteries of the (small cluster) QHAF spectrum such as low-energy singlets carrying unexpected quantum numbers [18] and exceptional sensitivity to small perturbations [34]. Experimentally, Kagome spin-1/2 systems generically contain small amounts of lattice and/or spin anisotropies [7] or even longer-range exchange interactions and the proximity to a QCP should render the experimental systems very sensitive to them. However, if under some conditions (pressure, chemical substitution,...) low-temperature spin-induced VBC order establishes, it could be revealed via small lattice modulations mediated by some magneto-elastic coupling. Lastly, we note that the above-mentioned perturbations as well as magnetic excitations [35] can be included in our scheme.

We acknowledge support from the French National Research Agency (ANR) and IDRIS (Orsay, France). D.P. thanks G. Misguich and A. Ralko for discussions.

- [5] P. Mendels et al., Phys. Rev. Lett. **98**, 077204 (2007).
- [6] A. Olariu et al., Phys. Rev. Lett. **100**, 087202 (2008).
- [7] A. Zorko et al., Phys. Rev. Lett. **101**, 026405 (2008).
- [8] J. Ruostekoski, Phys. Rev. Lett. **103**, 080406 (2009).
- [9] P. Lecheminant et al., Phys. Rev. B **56**, 2521 (1997).
- [10] P. Sindzingre et al., Phys. Rev. Lett. **84**, 2953 (1999).
- [11] H. C. Jiang, Z. Y. Weng, and D. N. Sheng, Phys. Rev. Lett. **101**, 117203 (2009).
- [12] P.W. Leung and Veit Elser, Phys. Rev. B **47**, 5459 (1993).
- [13] J. B. Marston and C. Zeng, J. Appl. Phys. **69**, 5962 (1991); SU(N) VBC have been introduced by N. Read and S. Sachdev, Phys. Rev. B **42**, 4568 (1990).
- [14] A. V. Syromyatnikov and S. V. Maleyev, Phys. Rev. B **66**, 132408 (2002).
- [15] P. Nikolic and T. Senthil, Phys. Rev. B **68**, 214415 (2003).
- [16] Ran Budnik and Assa Auerbach, Phys. Rev. Lett. **93**, 187205 (2004).
- [17] R.R.P. Singh and D.A. Huse, Phys. Rev. B **76**, 180407 (2007).
- [18] G. Misguich and P. Sindzingre, J. Phys. Cond. Matt. **19**, 145202 (2007).
- [19] D. Schwandt, M. Mambrini and D. Poilblanc, arXiv:1002.0774. The weights of higher-order resonances (involving 2 or more hexagons) decay rapidly with \mathcal{L} .
- [20] D.S. Rohksar and S.A. Kivelson, Phys. Rev. Lett. **61**, 2376 (1988).
- [21] Chen Zeng and Veit Elser, Phys. Rev. B **51**, 8318 (1995).
- [22] M. Mambrini and F. Mila, Eur. Phys. J. B **17**, 651 (2000).
- [23] For the frustrated QHAF on the square lattice see M. Mambrini, A. Läuchli, D. Poilblanc, and F. Mila, Phys. Rev. B **74**, 144422 (2006).
- [24] B. Sutherland, Phys. Rev. B **37**, 3786 (1988); N. Read and B. Chakraborty, Phys. Rev. B **40**, 7133 (1989).
- [25] For the same procedure on the frustrated QHAF on the square lattice see A. Ralko, M. Mambrini and D. Poilblanc, Phys. Rev. B **80**, 184427 (2009).
- [26] E.g. the IR of momenta K_{Γ} ($r_3 = r_2 = +$), K_B ($r_3 = +$) and K_A ($r_2 = +$) in TS^* [27] of the 108-site cluster ($\sigma = \pm$) contain 79 548 096, 159 073 536 and 238 642 176 fully symmetrized states, respectively. Other momenta (with larger Hilbert spaces) have not been considered. However, apart from K_C , they should not be involved in the GS manifold (see Table I).
- [27] Studied dimer liquids and VBC belong to the $\{0, 0, 0\}$ $\{1, 1, 1\}$ TS of the 48-site [108-site] cluster, named as TS^* . "Other TS" refers to the 3 other (degenerate) TS.
- [28] As the fidelity, this quantity is a useful tool to identify quantum phase transitions. See S. Chen, L. Wang, Y. Hao and Y. Wang, Phys. Rev. A **77**, 032111 (2008).
- [29] G. Misguich, D. Serban, and V. Pasquier, Phys. Rev. Lett. **89**, 137202 (2002).
- [30] R. Moessner and S. L. Sondhi, Phys. Rev. Lett. **86**, 1881 (2001).
- [31] A. Ralko et al., Phys. Rev. B **76**, 140404 (2007).
- [32] Reversely, the $\mathcal{N} = 48$ cell does not fit in the 108-site cluster. The $3 \times 4\sqrt{3} \times 4\sqrt{3}$ cluster (144 sites) which can accommodate both $\mathcal{N} = 36$ and $\mathcal{N} = 48$ cells is out of reach.
- [33] C. Xu and S. Sachdev, Phys. Rev. B **79**, 064405 (2009).
- [34] P. Sindzingre and C. Lhuillier, Eur. Phys. Lett. **88**, 27009 (2009).
- [35] A. Ralko, F. Becca and D. Poilblanc, Phys. Rev. Lett. **101**, 117204 (2008).

- [1] J.T. Chalker, P.C.W. Holdsworth, E.F. Shender, Phys. Rev. Lett. **68**, 855 (1992).
- [2] For review see e.g. "Two-dimensional quantum antiferromagnets", G. Misguich & C. Lhuillier, in "Frustrated spin systems", Ed. H. T. Diep, World-Scientific (2005).
- [3] M. Hermele, Y. Ran, P. A. Lee, and X.-G. Wen, Phys. Rev. B **77**, 224413 (2008).
- [4] M. Shores, E. Nytka, B. Bartlett, and D. Nocera, J. Am. Chem. Soc. **127**, 13462 (2005).